Optical Stark and Zeeman Spectroscopy of Thorium Fluoride, ThF, and Thorium Chloride, ThCl

Journal:	*The Journal of Physical Chemistry*
Manuscript ID	jp-2018-11853y.R2
Manuscript Type:	Special Issue Article
Date Submitted by the Author:	19-Jan-2019
Complete List of Authors:	Nguyen, Duc-Trung; Arizona State University, School of Molecular Sciences Steimle, Timothy; Arizona State University, Chemistry Linton, Colan; University of New Brunswick, Physics Cheng, Lan; Johns Hopkins University,

Optical Stark and Zeeman Spectroscopy of Thorium Fluoride, ThF, and Thorium Chloride, ThCl

Duc-Trung Nguyen and Timothy Steimle*

School of Molecular Sciences, Arizona State University

Tempe, Arizona 85287-1604, U.S.A.

Colan Linton

Physics Department, University of New Brunswick

8 Bailey Drive, Fredericton, NB, E3B5A3, Canada

Lan Cheng

Department of Chemistry

The Johns Hopkins University

Baltimore, Maryland, 21218 U.S.A.

Last Modified: January 12, 2019, 2018

*Corresponding Author: Prof. T. C. Steimle, School of Molecular Sciences,

Arizona State University, Tempe, Arizona 85287-1604, Phone (480)965-3265; e-Mail: TSteimle@ASU.edu

ABSTRACT

Experimentally and theoretically determined magnetic and electric dipole moments, bond distances and vibrational spacings are used for a comparative study of the bonding in ThF and ThCl. Numerous bands in the visible electronic spectra between 16400 cm^{-1}-18800 cm^{-1} of supersonically cooled molecular beam samples have been detected using medium resolution ($\Delta\nu \approx 0.1 cm^{-1}$), two dimensional (2D) spectroscopy. High resolution ($\Delta\nu$ < 20 MHz) field-free, Stark, and Zeeman spectroscopy of the detected [18.6] Ω=3/2 – $X^2\Delta_{3/2}$ band of ThF near 538.4 nm and the [18.2] Ω=3/2 – $X^2\Delta_{3/2}$ band of ThCl near 551.0 nm have been recorded and analyzed. Stark shifts and splitting were analyzed to produce $|\vec{\mu}_{el}|$ values of 1.453(7) D and 0.588(9) D, for the $X\,^2\Delta_{3/2}$ and [18.6]Ω=3/2 states of ThF, respectively, and 2.022(35) D and 3.020(55) D, for the $X^2\Delta_{3/2}$ and [18.2]Ω=3/2 states of ThCl. Zeeman splittings and shifts were analyzed to produce g_e values of 1.038(4) and 1.079(4) for the $X^2\Delta_{3/2}$ and [18.6]Ω=3/2 states of ThF and 1.130(4) and 1.638(4) for the $X^2\Delta_{3/2}$and [18.2]Ω=3/2 states of ThCl. Analysis of g_e values demonstrate that the $X^2\Delta_{3/2}$ and [18.6]Ω=3/2 states of ThF and the $X\,^2\Delta_{3/2}$ state of ThCl are predominately $^2\Delta_{3/2}$ spin-orbit components, whereas the [18.2] Ω=3/2 state of ThCl is an admixture of $^2\Delta_{3/2}$ and $^2\Pi_{3/2}$ spin-orbit components. A molecular orbital description of the ground states is used to rationalize the observed $|\vec{\mu}_{el}|$ values for the ThX(X=F,Cl,O and S) series, and garner insight into the bonding mechanism. The dipole moments in the ground state of ThF and ThCl have been calculated using relativistic coupled-cluster methods. It is demonstrated that the systematic inclusion of electron-correlation contributions plays an essential role in obtaining accurate predictions for the dipole-moment values in ThF and ThCl.

I. INTRODUCTION

Discovering new element-specific ligands for the separation of the minor actinides from the chemically similar lanthanides present in the raffinate of the plutonium and uranium extraction (PUREX) process could improve the treatment of spent nuclear fuel (SNF)[1-5]. This area of chemistry is challenging from both the experimental side, where the toxicity, radioactivity and short lifetime of nuclides hinder studies, and the theoretical side, where relativistic effects, electron correlation, and a very high density of states need to be addressed. An improved chemical understanding of the actinide elements that are not easy to study experimentally critically depends upon the development of computational methodologies for modeling molecular properties and chemical reactions. The most effective means of assessing various emerging computational methodologies is by making a comparison between experimentally derived and computed properties for simple Th and U containing gas-phase molecules[6-7], which can be studied using high-resolution spectroscopy. Of particular chemical relevance is a comparison of permanent electric dipole moments, $\vec{\mu}_{el}$, which are the most direct gauge of bond polarity, and magnetic g-factors which are sensitive to the valence electron spin and orbital angular momenta coupling. Electric dipole moments are sensitive to the nature of the chemically relevant valence electrons and are often predicted *ab initio*, fostering the connection between theory and experiment. Although magnetic g-factors are not routinely predicted in electronic structure calculations, they can be readily estimated *a priori* using the theoretically predicted spin-orbit coupled eigenstate compositions. Such compositions are often predicted either by ligand field theory [8-9] or *ab initio*[10-12]. Specifically, in the commonly used Hund's case (a) basis, the effective g-factor $g_e = \Lambda + 2.002\Sigma$, where Λ and Σ are the molecular fixed projections of the electronic orbital and spin angular momenta, respectively. Knowing the ΛS-state composition of a specific observed Ω-state suffices to predict g_e [13-15]. In addition to providing benchmark properties, high-resolution gas-phase studies of Th and U molecules address the fundamental question concerning the extent and nature of 5*f* and 6*d* participation in actinide metal−ligand covalency[16], which impacts actinide/lanthanide separation chemistry.

Here we report on the determination of $|\vec{\mu}_{el}|$ values, magnetic g-factors, vibrational spacings, and bond distances for thorium fluoride, ThF, and thorium chloride, ThCl from the analysis of

electronic spectra recorded in the 16400 cm^{-1}-18800 cm^{-1} range. To a first approximation the ground and low-lying excited states of these very polar molecules can be understood by considering the ligand-field interaction of the $Th^+(7s^26d^1)$ and slightly more energetic[17] $Th^+(7s^16d^2)$ configurations. The $Th^+(7s^26d^1)$ gives rise to the $X^2\Delta_{3/2}$, $X^2\Delta_{5/2}$, $A^2\Pi_{1/2}$, $A^2\Pi_{3/2}$ and $B^2\Sigma^+$ states. The observed ground $|\Omega| = 3/2$ state is primarily the component of the $^2\Delta_r$ state (i.e. $X^2\Delta_{3/2}$) arising from the $Th^+(7s^26d^1)$ configuration. The low-lying excited $Th^+(7s^16d^2)$ configuration ligand-field splits into 90 additional strongly interacting states (45 Ω-doublets) of slightly higher energy. A particular goal of the present study is to determine if the observed properties of ThF and ThCl can be qualitatively understood via a ligand-field description and the difference between Cl and F. There should be subtle differences in bonding due to the more dispersed charge on the larger Cl^- anion as compared to the smaller F^- anion. In addition the longer bond distance of ThCl results in a weaker electrostatic repulsion causing less of a bifurcation of the states arising from the $Th^+(7s^26d^1)$ and $Th^+(7s^16d^2)$ configuration[17].

The work reported here was greatly aided by the previous combined experimental and theoretical studies on the ThF/ThF^+ system[10] and more recently on the $ThCl/ThCl^+$ system[12]. In the earlier study the electronic spectrum of ThF in the 19,500–21,300 cm^{-1} spectral range was investigated and supporting electronic structure calculations performed[10]. The mass-selected resonance enhanced multi-photon ionization (REMPI) spectrum was recorded and analyzed. Three bands that appeared in the REMPI spectrum were subsequently recorded using medium resolution ($\Delta\nu$~0.05 cm^{-1}) laser-induced fluorescence (LIF) detection. The fine structure was analyzed to determine a rotational constant, B_0, of 0.237(5) cm^{-1} for the assigned $X^2\Delta_{3/2}$ state. Dispersed fluorescence from two bands was recorded and analyzed to give the ground state vibrational spacing, $\Delta G_{1/2}$, of 605(15) cm^{-1} and the energy for the $X^2\Delta_{5/2}$ spin-orbit component of 2575 cm^{-1}. Multi-reference configuration interaction (MRCI) and couple cluster calculations predicted B_0 and $\Delta G_{1/2}$ values for the $X^2\Delta_{3/2}$ state of 0.2264 cm^{-1} and 574 cm^{-1}, respectively, and a dominant $Th^+(7s^26d^1)F^-(2p^6)$ configuration. The predicted term energies for the $A^2\Pi_{1/2}$ and $A^2\Pi_{3/2}$ states arising from the $Th^+(7s^26d^1)$ configuration were 4253 and 6134 cm^{-1}, respectively. In the more recent study[12] of $ThCl/ThCl^+$, the low resolution LIF spectrum in the 18,100 - 25,000 cm^{-1} range was recorded and numerous observed bands were confirmed to be associated with ThCl using mass-selected REMPI spectroscopy. Intense bands near 21,977.6 and 23,507.9 cm^{-1} were further

studied at moderate resolution using LIF excitation and dispersed fluorescence spectroscopy. The analysis of those spectra determined, amongst other things B_0 and $\Delta G_{1/2}$ values of 0.08899(18) cm^{-1} and 341(14) cm^{-1}, respectively, for the $X^2\Delta_{3/2}$ state and term energies of 3498, 4075, and 4361 cm^{-1} for low-lying excited states assigned as $X^2\Delta_{5/2}$, $^4\Phi_{3/2}$ and $^2\Pi_{3/2}$, respectively. The low-lying ΛS excited states were mapped using a complete active space self-consistent field (CASSCF) which was followed by second-order perturbation theory calculations to predict the energies and the nature of the low-lying Ω-states. The leading contributions to the spin-orbit coupled eigenstates in terms of the ΛS basis states were given from which predicted g_e values can be obtained (see below). Predicted values for $\vec{\mu}_{el}$ were not reported as part of either of the combined theoretical and experimental studies of ThF and ThCl.

At approximately the same time of the aforementioned ThF/ThF^+ study, the results of both relativistic and non-relativistic electronic structure predictions for ThF_x(x=1-4) were reported[18]. The relativistic four-component calculations performed using the Dirac-Coulomb Hamiltonian predicted term energizers for the $X^2\Delta_{3/2}$, $X^2\Delta_{5/2}$, $A^2\Pi_{1/2}$, $A^2\Pi_{3/2}$, $a^4\Sigma^-_{1/2}$ and $a^4\Sigma^-_{3/2}$ states of 0, 2415, 3132, 6099, 6124 and 6911 cm^{-1}, respectively. The leading contributions to the spin-orbit coupled eigenstates, in terms of the ΛS basis states, were not given. The non-relativistic calculation predicted $\Delta G_{1/2}$ values 604 and 571 cm^{-1} for the $X^2\Delta_r$ and $a^4\Sigma^-$ states. More recently, the infrared absorption spectra of argon and neon matrix isolated samples of ThF have been reported[19]. As part of that study, supporting electronic structure predictions at the coupled cluster with singles and doubles with a perturbative triples correction (CCSD(T)) were also performed. The observed $X^2\Delta_{3/2}$, $\Delta G_{1/2}$ values were consistent with the CCSD(T) predicted value of 598.9 cm^{-1}. Although no prediction of $\vec{\mu}_{el}$ was reported, the natural bond order analysis predicted a charge distribution of $Th^{+0.7}F^{-0.7}$ and an electron configuration population of Th($7s^{1.86}7p^{0.03}6d^{1.15}$ $1f^{0.26}$) for the $X^2\Delta_{3/2}$ state.

II. EXPERIMENTAL SECTION

The laser ablation-reaction supersonic expansion production scheme was similar to that used in the previous studies of ThO[20-21] and ThS[22-23], but with the expansion gas being a 95%Ar/5% CF_4 mixture in the case of ThF or Ar passed over a room temperature sample of CCl_4 in the case of ThCl. The relatively high backing pressure (~4000 kPa) and low 532 nm ablation

energy flux (~10 mJ/pulse and 1/2 m focal length lens) resulted in a rotational temperature of approximately 10 K. Initial searches were performed using a moderate resolution, two-dimensional (2D) spectroscopic technique[24-25] similar to that performed for ThO[20]. In these measurements the free-jet expansion was probed approximately 10 cm from the ablation source. The 2D spectra were created by stepping the pulsed dye laser wavelength in 0.2 cm^{-1} increments and capturing a 75 nm wide spectral region of the dispersed laser induced fluorescence (DLIF) for each laser excitation wavelength. The fluorescence was directed into a ¾ meter, low f-number (6.2), monochromator and detected with a cooled gated intensified charge coupled detector (ICCD). Typically, 20 laser ablation samples were averaged at each pulsed dye laser wavelength. The entrance slit width of the monochromator was set to 2 mm resulting in an approximately ±4 nm spectral resolution for the DLIF signal of the 2D spectra. Higher resolution DLIF were subsequently recorded by tuning the pulsed dye laser wavelength to a resonant wavelength and narrowing the entrance slit of the monochromator slits to approximately 1 mm. Typically 10000 laser ablation samples were averaged for the higher resolution DLIF spectroscopy.

An intense band of ThF near 538.4 nm, assigned as the [18.6] Ω=3/2 – $X\,^2\Delta_{3/2}$(v′,0) transition, and an intense band of ThCl near 551.0 nm, assigned as the [18.2] Ω=3/2 – $X^2\Delta_{3/2}$ (v′,0) transition, were subsequently studied using high-resolution, single frequency, field-free, Stark and Zeeman spectroscopy. The experimental set-up for these measurements was similar to that used in the previous high-resolution study of ThO[21]. The output of the free-jet expansion was skimmed to produce a well-collimated molecular beam, which was crossed with the cw-dye laser radiation at approximately 1/2 m from the source. The fluorescence was monitored off resonance through a ±10 nm bandpass filter centered at 570 nm and 560 nm for ThF and ThCl, respectively. The fluorescence was detected with a cooled photomultiplier tube (PMT) and the signal processed using photon-counting techniques. For the Stark measurements, the static electric field was generated by application of a voltage to a pair of conducting neutral density filters that straddle the intersection of the laser beam and molecular beam. For the Zeeman measurements, a homogeneous magnetic field was produced by attaching rare-earth magnets to a homemade magnetic yoke. The magnetic field was measured using a commercial Hall-type probe, and the electric field was determined by measuring the voltage and plate spacing. The systematic errors due to the electric field strength calibration and uncertainties in spectral shift measurements were estimated to be less than 2%.

III. COMPUTATION DETAILS

Relativistic coupled-cluster calculations have been performed in order to obtain accurate predictions for the ground-state dipole-moment values of ThF and ThCl. Excited state properties were not predicted. The CCSD(T)[26] method together with the exact two-component Hamiltonian using atomic mean-field spin-orbit integrals (the X2CAMF Hamiltonian) has been used to obtain consistent treatments of scalar-relativistic, spin-orbit (SO), and electron-correlation effects. The X2CAMF[27] approach combines the X2C theory[28-30] for decoupling the electronic and positronic degrees of freedom with the atomic mean-field approach[31] for efficiently treating two-electron SO contributions. It has been shown to provide accurate results in calculations of dipole moments in heavy-element containing systems in comparison with the fully relativistic Dirac-Coulomb approach. The ANO-RCC basis sets[32-33], have been used in the fully uncontracted form in these X2CAMF-CC calculations. The uncontracted ANO-RCC sets are of augmented triple-zeta quality and also include core correlating functions. The X2CAMF-CCSD(T) calculations presented here have correlated the 2*s* and 2*p* electrons of fluorine, the 2*s*, 2*p*, 3*s*, and 3*p* electrons of chlorine, and the 5*s*, 5*p*, 5*d*, 6*s*, 6*p*, 7*s*, and 6*d* electrons of thorium together with the virtual spinors with energies below 1000 Hartree in ThF and those below 100 Hartree in ThCl, i.e., 37 electrons/679 virtual spinors for ThF and 45 electrons/602 virtual spinors for ThCl. These SO-CCSD(T) calculations with the correlation of the sub-valence electrons and extensive virtual spaces have been enabled by the recent development of the semi-atomic-orbital based algorithm for the SO-CCSD(T) method[34].

The high-level correlation contributions [those beyond CCSD(T)] are often significant for computed molecular properties. Due to the high computational costs of the CC singles doubles triples (CCSDT) method[35-36] and the CCSDT with the non-iterative inclusion of quadruple excitations [CCSDT(Q)] method[37], these corrections have been obtained from scalar-relativistic calculations using relatively small basis sets with only the valence electrons correlated. The spin-free X2C in its one-electron variant (SFX2C-1e) scheme[38-40] together with the corresponding triple-zeta correlation-consistent basis sets (cc-pVTZ-X2C)[41-42] have been used here. The full triples contributions have been obtained as the difference between SFX2C-1e-CCSDT and SFX2C-1e-CCSD(T) results, while the quadruples contributions as the difference between SFX2C-1e-CCSDT(Q) and SFX2C-1e-CCSDT values. The 2*s* and 2*p* electrons of fluorine, the 3*s*

and 3*p* electrons of chlorine, and the 6*s*, 6*p*, 7*s*, and 6*d* electrons of Th (19 electrons for both ThF and ThCl) have been correlated in these calculations.

In all calculations presented here, the dipole-moment values have been obtained by means of finite difference of energies. The simple two-point formula has been employed with a field strength of 0.001 a.u.. Tight convergence thresholds have been used in the Hartree-Fock and CC calculations. Upon convergence, the variation of coupled-cluster energies is below 10^{-9} Hartree. All calculations have been carried out using the CFOUR program[43-45] except that the CCSDT and CCSDT(Q) calculations have been performed using the MRCC program[46-48].

IV. OBSERVATIONS

The 2D spectrum of the products generated via ablation of thorium with the CF_4/argon mixture in the range of 17,400 to 18,800 cm^{-1} is presented in Figure 1. The monochromator is tracked with the laser excitation wavelength which is therefore always at the center of the 75 nm spectral window of the DLIF spectrum. At the beginning of the scan (i.e. 17,400 cm^{-1}) the central DLIF wavelength is approximately 590 nm and at the end of the scan (i.e.18,800 cm^{-1}) it is approximately 545 nm. The horizontal bands of fluorescence are the excitation spectra monitored either on resonance, to higher frequency (Stokes), or to lower frequency (anti-Stokes) than that of the laser. There are eight band systems evident from inspection of the DLIF and are indicated by the vertical slices labeled D1 to D8 in Figure 1. D8 is readily assigned to ThO emission resulting from the excitation of the $F^1\Sigma^+ - X^1\Sigma^+(0,0)$ (ν=18313 cm^{-1}) band because it exhibits emission shifted from the excitation laser by the known vibrational spacing[49] of 895 cm^{-1} (Stokes 2). The diagonal stripe of fluorescence, which appears at 546.1 nm in the DLIF, is an artifact associated with emission from the very intense ThO $F^1\Sigma^+ - X^1\Sigma^+(0,0)$ band excited by amplified stimulated emission (ASE) of pulsed dye laser. This band fluoresces predominantly on resonance and hence the diagonal stripe of fluorescence crosses the on-resonance excitation signal at 18,313 cm^{-1}. D1 to D7 exhibit features shifted by approximately 600 cm^{-1} (Stokes 1) and 1200 cm^{-1} (Stokes 3) to the red of the excitation spectrum and are readily assigned to ThF excited state emission down to either v″=1 and v″=2 of the $X^2\Delta_{3/2}$ state. With the exception of D4, which exhibits an anti-Stokes component, the transitions are excitation from the $X^2\Delta_{3/2}$(v=0) level to multiple excited electronic states. Hence the bands at 17712, 17790, 17864, 18030, 18295, 18360 and 18575 cm^{-1} are assigned

to ThF. Additional bands of ThF at 16335, 16364, 16527 and 16564 cm^{-1} were observed in the 16400 cm^{-1}-18800 cm^{-1} spectral range probed.

Higher resolution DLIF spectra resulting from pulsed laser excitation of the band heads at 17712, 17865 and 18575 cm^{-1} are presented in Figure 2. It is evident that the band at 17712 cm^{-1} is an excitation from the $X^2\Delta_{3/2}$ (v″=1) state due to presence of an anti-Stokes feature. In addition to emission to excited vibrational levels of the $X^2\Delta_{3/2}$ state, emission to the $X^2\Delta_{5/2}$ state and the heretofore unobserved $A\,^2\Pi_{1/2}$ state are observed. The measured $\Delta G_{v+1/2}$ spacings for the $X^2\Delta_{3/2}$ state were determined to be 595.6, 594.4, 591.5 and 589.1 cm^{-1} for v=0, 1, 2 and 3, respectively. A linear least squares fit of these values to the standard expression for vibrational spacing gives ω_e (600.6±4 cm^{-1}) and $\omega_e x_e$ (1.2 ± 1/2 cm^{-1}) for the $X^2\Delta_{3/2}$ state, which compare well with the previously determined[10] ω_e value of 605(15) cm^{-1}. High-resolution field-free, Stark and Zeeman measurements were performed only on the intense 18575 cm^{-1} band.

The pulse dye laser excitation spectrum in the range of 18,555 to 18,585 cm^{-1} extracted from the "Stokes 3" horizontal slice of a 2D spectrum recorded using a laser step size of 0.1 cm^{-1} is presented in the top panel of Figure 3. The *P*, *Q* and *R* branches are evident. The 18,572.5 to 18,576.5 cm^{-1} portion of this band recorded using the single frequency cw-dye laser excitation and a skimmed molecular beam is presented in the lower panel of Figure 3. In this case, the fluorescence was viewed off-resonance through a 570 nm ±10 nm bandpass filter and processed with photon counting. The branch features have a full width half maximum (FWHM) of approximately 15 MHz. Guided by the previously determined[10] B_0'' (=0.237(5) cm^{-1}) and a reasonable estimate for B_0', the quantum number assignment of the branch features was straightforward. The observation of the lowest branch features (*R*(3/2), *Q*(3/2) and *P*(5/2)) makes the Ω=3/2 assignment of the excited state unquestionable and the band is assigned as the [18.6] Ω=3/2 – $X^2\Delta_{3/2}$(v′,0) transition. There is no evidence of ^{19}F(I=1/2) hyperfine splitting or Ω-doubling. Each level of both the [18.6] Ω=3/2 and $X^2\Delta_{3/2}$ (v=0) states is a nearly degenerate pair of opposite parity. The branch assignments were confirmed by the Zeeman and Stark measurements (see below). The precisely measured transition frequencies of 24 branch features along with the assignments and residuals are presented in Table 1 of the Supporting Information.

Stark spectra for the $R(3/2)$ (ν=18575.4762 cm^{-1}) and $Q(3/2)$ (ν=18575.4900 cm^{-1}) lines were measured at fields up to 1500 V/cm. Spectra of the $R(3/2)$ line, recorded field-free and with the laser polarized parallel (ΔM_J =0) perpendicular (ΔM_J =±1) to a 1500 V/cm electric field, are presented in Figure 4. The spectrum exhibits a very nearly linear Stark tuning consisting of four components for parallel polarization, confirming the quantum number assignment and the negligibly small Ω-doubling. Also presented in Figure 4 are the energy levels obtained using the optimized parameters and quantum number assignments. The 52 precisely measured Stark shifts along with quantum number assignments and residuals are presented in Table 2 of Supporting Information. Zeeman spectra for the $R(3/2)$, $Q(3/2)$ and $Q(5/2)$ (ν=18574.3117cm^{-1}) lines were measured at a field of 876 G. The $R(3/2)$ line recorded field-free and with parallel (ΔM_J =0) and perpendicular (ΔM_J =±1) polarizations are presented in Figure 5. The Zeeman shifts are very nearly symmetrically spaced around the field-free feature, indicating negligible second-order contributions. Also presented are the predicted spectra and associated energy levels obtained using the optimized parameters. The 34 precisely measured Zeeman shifts along with quantum number assignments and residuals are presented in Table 3 of Supporting Information.

The pulse dye laser excitation spectrum of the ablated Th/CCl_4 reaction products in the range of 18,050 to 18,250 cm^{-1} is presented in the top panel of Figure 6. The spectrum was extracted from the on-resonance horizontal slice of a 2D spectrum. This is the only band of ThCl observed in the 16,400 cm^{-1}-18,800 cm^{-1} range surveyed using 2D spectroscopy. The density of states for the ThCl is likely to be similar that of ThF and the paucity of observed transitions for ThCl relative to that of ThF is likely due to the less efficient production of ThCl relative to that of ThF. The strong feature near 18180 cm^{-1} is the fluorescence resulting from excitation of the $^2P_0$ ($6d^27s^2$, E=2558.1 cm^{-1}) to a J=0 level (E= 20737.3cm^{-1}) of Th atoms. The DLIF spectrum resulting from excitation near the band head at 18158 cm^{-1} is presented in Figure 7. The measured $\Delta G_{1/2}$ and $\Delta G_{3/2}$ spacings are consistent with the previously determined[12] ω_e = 341(14) cm^{-1}. The 18,154.8 to 18,558.3 cm^{-1} portion of this band recorded using the cw-dye laser excitation is presented in the lower panel of Figure 6. There is no evidence of splitting arising from the ^{35}Cl(I=3/2) or ^{37}Cl(I=3/2) magnetic and nuclear electric quadrupole hyperfine interactions. Unlike ThF, there is considerable Ω-doubling which has an approximate J^3 dependence. The splitting in the $R(J\text{-}1)$, $Q(J)$ and $P(J\text{+}1)$ lines were all identical which showed that the splitting was solely due

to excited state Ω-doubling. The spectra of both isotopologues, $Th^{35}Cl$ and $Th^{37}Cl$, were readily assigned using combination differences. The observation of the lowest branch features shows that Ω=3/2 in both ground and excited state and the band is assigned as the [18.2] Ω=3/2 – $X^2\Delta_{3/2}$(v′,0) transition. The precisely measured transition frequencies of 80 branch features of $Th^{35}Cl$ and 46 of $Th^{37}Cl$, along with the assignments and residuals are presented in Tables 4 and 5 of the Supporting Information.

The Stark effect in the partially resolved R_a(3/2) (ν=18157.1306 cm^{-1}) and R_b(3/2) (ν=18157.1310 cm^{-1}) lines, and the unresolved Q(3/2) (ν=18156.7075 cm^{-1}) lines of $Th^{35}Cl$ were measured at fields up to 1013 V/cm. Stark spectra of the Q(3/2) line recorded in the presence of a 405 V/cm electric field are presented in Figure 8. There is a slight asymmetric shift of the Stark spectra to lower wavenumbers. Also shown in Figure 8 are the associated energy levels and assignment. The 33 precisely measured Stark shifts along with quantum number assignments and residuals are presented in Table 6 of Supporting Information. Zeeman spectra for the R_a(3/2), R_b(3/2), and unresolved Q(3/2) and P(3/2) (ν=18156.2643 cm^{-1}) lines were recorded at fields of 452G and 931G. The Zeeman spectra of the P(3/2) line, recorded field-free and in the presence of a 931G field with parallel and perpendicular polarization are presented in Figure 9. There is a slight asymmetric shift to the low wavenumbers. The 55 precisely measured Zeeman shifts along with quantum number assignments and residuals are presented in Table 7 of Supporting Information.

V. ANALYSIS

The [18.6] Ω=3/2 – $X^2\Delta_{3/2}$ band of ThF and the [18.2] Ω=3/2 – $X^2\Delta_{3/2}$ band of ThCl are free of local perturbations. The $X^2\Delta$ states of both molecules are in the Hund's case(a) coupling limit with an observed spin-orbit splitting[10, 12] reported to be 2575 cm^{-1} and 3498 cm^{-1} for ThF and ThCl, respectively. For the analysis performed here it was assumed that the [18.6] Ω=3/2 and [18.2] Ω=3/2 states were also components of $^2\Delta$ states with identical spin-orbit splitting to the ground state counterparts. This Hund's case(a) picture assists in making a spectral simulations and analyses. The effective Hamiltonian operator used to model the energies and wave functions of these $^2\Delta$ states consisted of spin-orbit, rotational, and Ω-doubling terms[50]:

$$\hat{H}^{eff} = T_v + A\hat{L}_z\hat{S}_z + B(\hat{J}-\hat{L}-\hat{S})^2 - \frac{1}{2}(p_\Delta + 4q_\Delta)(\hat{S}_+\hat{J}_+^3 + \hat{S}_-\hat{J}_-^3), \quad 1)$$

where the rotational term has been written in the $\boldsymbol{R}^2$ –form, $\hat{R} \equiv (\hat{J} - \hat{L} - \hat{S})$. The Ω-doubling term is written in terms of the raising and lowering operators. A 4×4 matrix representation was constructed in a non-parity conserving Hund's case (a) basis set, $\Psi(case(a)) = \left|\eta\Lambda; S\Sigma; J\Omega M_J\right\rangle$, and diagonalized to produce predicted field-free energies and eigenvectors. The matrix elements were taken from Ref. [50]. The spin-orbit parameters, A, for the $X^2\Delta$ states, as well as those for the excited $^2\Delta$ states, were constrained to 1287.5 cm^{-1} for ThF and 1749 cm^{-1} for ThCl, as given from the previously measured[10, 12] separation between the $X^2\Delta_{3/2}$ and $X^2\Delta_{5/2}$ states. The observed transition wavenumbers were used as input to a non-linear least squares fitting procedure to produce the optimized set of T_v, B and $(p_\Delta+4q_\Delta)$ values and associated errors and are presented in Tables 1 and 2. The standard deviation of the fits were 0.0003 cm^{-1}, 0.0008 cm^{-1} and 0.0006 cm^{-1} for ThF, Th^{35}Cl and Th^{37}Cl, respectively. The slightly larger rms for ThCl is consistent with the poorer signal to noise.

The Stark and Zeeman interactions were modelled using standard effective Hamiltonian operators[51]:

$$\hat{H}^{Stark} = -\hat{\mu}_{el}\mathbf{g}\hat{E} \qquad 2)$$

and

$$\hat{H}^{Zee} = \hat{\mu}_m\mathbf{g}\hat{B} \approx g_L\mu_B B_z\hat{L}_Z + g_S\mu_B\hat{S}_Z B_z\,. \qquad 3)$$

The data are only sensitive to the magnitude of the electric dipole moment, $|\mu_{el}|$. The small magnetic moments associated with rotation and nuclear spin were neglected as were the anisotropic corrections to the electron spin Zeeman term[51]. In the effective Hamiltonian approach used here, the electronic orbital and spin g-factors, g_L and g_S, are considered variables and not constrained to the free-electron values of 1.000 and 2.002, respectively. Because the data are restricted to only one spin-orbit component of the $^2\Delta$ states, only g_L or g_S can be determined. Based upon previous experience[52], it was decided to constrain g_S to the free electron value of 2.002 and use g_L as the fitting parameter. The deviation of the fitted g_L value from unity is a reflection of the departure of the states from $^2\Delta$ character.

Initial analyses of the observed Stark and Zeeman shifts were performed using the simple expressions derived from degenerate perturbation theory[51]. The residuals of those fits exhibited

small systematic trends and a more complete matrix representation approach was employed in the final analysis. Specifically, a matrix representation constructed using the Hund's case (a) basis associated with J=1/2 through 8.5 was constructed and diagonalized to produce eigenvalues and eigenvectors. The truncation of the infinite dimension matrix representation at J=8.5 introduces error well below the uncertainty in the experimental measurements. For the Stark measurements the standard deviation of the fits were 7 and 9 MHz for ThF and ThCl, respectively. For the Zeeman measurements the standard deviation of the fits were 10 and 11 MHz for ThF and ThCl, respectively. The slightly higher standard deviation for ThCl is consistent with the poorer signal to noise. The determined $|\mu_{el}|$ and g_L values and associated errors are presented in Tables 1 and 2.

VI. DISCUSSION

Analysis of the DLIF spectra of ThF (Figure 2) produces ground vibrational parameters (ω_e=600.6±4.0 cm^{-1}, $\omega_e x_e$ =1.2 ± 0.5cm^{-1}) and a T_0 (for the $X^2\Delta_{5/2}$ state (=2593 ± 10 cm^{-1}), which are slightly more precise than the previous values[10]. The ThF DLIF spectra also exhibit features that are displaced from the laser (Figure 2) by 3158± 10 cm^{-1} and 4130 ± 10 cm^{-1}, which are emission to low-lying excited states. The MRCI + SO-CI predicted values[10] for the $X^2\Delta_{3/2}$, $X^2\Delta_{5/2}$, $A^2\Pi_{1/2}$ and $A^2\Pi_{3/2}$ states arising from the $Th^+(7s^26d^1)$ configuration are 0, 1939, 4253, and 6134 cm^{-1}, respectively, whereas the four-component relativistic calculation prediction[18] gives 0, 2415 3132, and 6099 cm^{-1}, respectively. Given the better agreement of the four-component relativistic calculation for $T_0(X^2\Delta_{5/2})$(2582 ± 10 cm^{-1} *vs* 2415 cm^{-1}), it is reasonable to assign the observed 3158 cm^{-1} to the $A^2\Pi_{1/2}$ state. Emission to the $A^2\Pi_{3/2}$ state is too red shifted for detection with the ICCD. Excitation of the 17865 cm^{-1} band produces stronger emission to the $A^2\Pi_{1/2}$ state than excitation of either the 18575 or 17712 band suggesting that excited state associated with the 17865 cm^{-1} band most likely has Ω=1/2. This assignment also explains the absence of emission to the X $^2\Delta_{5/2}$ state in the 17865 cm^{-1} band DLIF spectrum.

The rotational analysis for both isotopologues of ThCl was straightforward with no evidence of local perturbations. The ratio of the rotational constants, $B(Th^{35}Cl)/B(Th^{37}Cl)$, is 1.0493 for the ground state and 1.0481 for the excited state. The ratio of the reduced masses is 1.0493 so the ground state in particular is very well behaved and the ratio for the excited state is close to the theoretical value. Analysis of the DLIF spectra of ThCl (Figure 7) produces ground

vibrational spacings that are consistent with the previously obtained values of ω_e =342.3± 1.4 cm^{-1} and $\omega_e x_e$ =1.02. The vibrational isotope shift for T_0 combined with the ground state vibrational constants gives an ω_e for the [18.2] Ω=3/2 state of approximately 338 cm^{-1}. The DLIF spectrum for ThCl (Figure 7) exhibits features shifted from the laser by 1670 ± 15, 1989 ± 15 and 2390 ± 15 cm^{-1}, in addition to features associated with vibrational progression to the $X\ ^2\Delta_{3/2}$ state. Interestingly the DLIF does not exhibit a feature shifted from the laser by 3498 cm^{-1}, which was previously observed and assigned to emission to the $X^2\Delta_{5/2}$ state. The predicted[12] energies for the $X^2\Delta_{3/2}$, $X^2\Delta_{5/2}$, $A^2\Pi_{1/2}$, and $A^2\Pi_{3/2}$ states arising from the Th$^+$($7s^2 6d^1$) configuration are 0, 3050, 1820, and 4288 cm^{-1}, respectively. In addition, $^4\Phi_{3/2}$, $^4\Phi_{5/2}$, $^4\Sigma_{1/2}$, and $^4\Sigma_{3/2}$ states from the Th$^+$($7s^1 6d^2$) configuration are predicted at 3641, 5198, 4107, and 4796 cm^{-1}, respectively. Note that there is less of a bifurcation of the states arising from the Th$^+$($7s^2 6d^1$) and Th$^+$($7s^1 6d^2$) configuration for ThCl than in ThF because of the longer bond distance which results in a weaker electrostatic repulsion[17]. The observed features shifted by 1670 ± 15 and 1989 ± 15 cm^{-1} relative to the laser are assigned as emission to the v = 0 and 1 levels of the $A^2\Pi_{1/2}$ state. The feature shifted by 2390 ± 15 cm^{-1} is assigned as emission to the v=0 level of the $X^2\Delta_{5/2}$ state which would make the spin-orbit splitting in the $X^2\Delta$ state of ThF (2582 ± 10 cm^{-1}) comparable to that of ThCl (2390 ± 15 cm^{-1}) .

The computed dipole-moments for the ground state of ThF and ThCl are summarized and compared with the corresponding experimental values in Table 3. All predicted values are much less than the approximate 6D expected for a Th^{+1} F^{-1} or Th^{+1} Cl^{-1} charge distribution due to the induced dipole of the back polarized non-bonding 7*s* electrons. The induced dipole moment associated with polarization of the Th-metal centered electrons opposes that of the primary moment. At the Hartree-Fock level of prediction (X2CAMF-HF) the μ_{el} values for ThF and ThCl are -0.018D and 0.645D with the negative sign indicating a Th$^{\delta-}$F$^{\delta+}$ charge distribution. Upon inclusion of electron correlation the predicted μ_{el} changes sign in the case of ThF and values for both ThF and ThCl increase in magnitude. Electron correlation accounts for the contribution from the Th$^+$($7s^1 6d^2$) configuration to the description of the $X\ ^2\Delta_{3/2}$ states. The 6*d* orbital of this configuration is more contracted and less back-polarized than the 7*s* orbital and hence the induced dipole is reduced upon inclusion of electron correlation.

The X2CAMF-CCSD(T) results agree reasonably well with experiment. They overestimate the dipole-moment values by about 3.5% in the case of ThF and about 11% in the

case of ThCl. The column "ΔT" of Table 3 contains the differences between SFX2C-1e-CCSDT and SFX2C-1e-CCSD(T) results, while the "+ΔQ" column contains the differences between SFX2C-1e-CCSDT(Q) and SFX2C-1e-CCSDT results. The uncontracted ANO-RCC basis sets have been used in X2CAMF-CCSD(T) calculations. The cc-pVTZ-X2C basis sets have been employed to obtain high-level correlation contributions. The inclusion of triples and quadruples contributions improves the agreement between the calculation and experiment. Note that both the full triples contributions and the quadruples corrections reduce the magnitude of dipole moments, namely, the cancellation between these two types of contributions, which prevails in calculations of thermochemical parameters, have not been observed in the present calculations of dipole moments. Consequently, it is necessary to include these high-level correlation contributions in order to obtain nearly quantitative agreement between the calculations and the experiment.

The experimentally measured dipole moments are compared with those of other thorium containing molecules and UF in Table 4. Also presented are equilibrium bond distances, R_e, the reduced dipole moments, $\mu_{el}^{Red.} \equiv |\mu_{el}| / R_e$, which focuses on the electronic contribution, the effective nuclear charge, q^{eff}, and the difference of the Pauling electro-negativities of F, Cl, O, and S and those of the metal. The effective nuclear charge is the equivalent point charge at the bond length separation required to reproduce the observed $|\vec{\mu}_{el}|$ values. The bond lengths for ThF and ThCl are from the current study and those for ThO, ThS, and UF from Ref.[53], Ref.[22] and Ref[15], respectively. The ordering of $\mu_{el}^{Red.}$ and q^{eff} values amongst isovalent molecule are ThF < ThCl and ThO < ThS, which is contrary to that of the electronegativity differences which are ThF > ThCl and ThO > ThS. This is understood by considering the dominant configurations, which are given in Table 4, and polarization of the Th-metal centered electrons. Each of these four molecules has two electrons in the 7*s* orbital which readily hybridizes to shift the electron density away from the electrophilic ligand center. The longer bond distance, and hence smaller hybridization, causes the induced dipole moments in ThS and ThCl to be smaller than that for ThF and ThO resulting in $\mu_{el}^{Red.}$ and q^{eff} for ThF and ThO being smaller than those for ThS and ThCl.

Similarly, the relative values of $\mu_{el}^{Red.}$ for ThF and UF are inconsistent with simple electrostatic arguments. Specifically, $\mu_{el}^{Red.}$ for ThF (0.7026 D/ Å) is considerably smaller than that for UF (0.99D/ Å) even though the difference in electronegativities of Th and F (2.68) is larger

than that of U and F (2.60). Both q^{eff} for ThF (0.146e) and UF (0.206e) are considerably smaller than the expected 1.0e value due to the polarization of the doubly occupied 7*s* orbital. Given the nearly identical bond distances of UF and ThF, it is expected that the large induced dipole moments due to the back polarization of the 7*s* electrons should be comparable in the two molecules. A qualitative rationalization for the ordering of $\mu_{el}^{Red.}$ and q^{eff} can be realized by considering the other valence electrons. Near the equilibrium distance the ground state wave function of UF is predicted[7] to be almost entirely of $5f^3\,7s^2$ character, with the leading spin−orbit contributions of 80.74% $^4I_{4.5}$ + 16.50% $^4H_{4.5}$ + 2.54% $^4\Gamma_{4.5}$. The $X\,^2\Delta_{3/2}$ state of ThF is almost entirely of $7s^2 6d^1$ character. The more diffuse and polarizable 6*d* orbital of ThF makes a larger contribution to the opposing induced dipole moment relative to that produced by the contracted, less polarizable 5*f* orbital of UF causing $\mu_{el}^{Red.}$ for ThF (0.7026 D/ Å) to be considerably smaller than that for UF (0.99 D/ Å).

In the Hund's case (a) effective Hamiltonian approach used here $g_e = g_L\Lambda + g_S\Sigma$ with g_L and g_S treated as variables to account for mixing of electronic states. Using the fit g_L values of Tables 1 and 2 and assuming that $g_S = 2.002$ then the determined g_e values are 1.075(4) and 1.156(4) for the $X\,^2\Delta_{3/2}$ and [18.6]Ω=3/2 states of ThF and 1.130(4) and 1.638(4) for the $X\,^2\Delta_{3/2}$ and [18.2]Ω=3/2 states of ThCl. For an isolated pure Hund's case (a) $^2\Delta_{3/2}$ state $g_e = 0.9988$ and for a $^2\Pi_{3/2}$ state $g_e = 2.0011$. The observed g_e values can be reproduced by assuming that the $X^2\Delta_{3/2}$ and [18.6] Ω=3/2 states of ThF and the $X\,^2\Delta_{3/2}$ and [18.2]Ω=3/2 states of ThCl are composed of 7%, 15%, 13%, and 64% $^2\Pi_{3/2}$ character, respectively. The larger deviation from the $X^2\Delta_{3/2}$ description for ThCl as compared to ThF (13% *vs* 7%) is most likely due to the larger contribution of the $Th^+(7s^1 6d^2)$ configuration for ThCl than for ThF . The ground state of ThCl is predicted[12] to be 92% $^2\Delta_{3/2}$ and 7% $^2\Pi_{3/2}$, significantly different from the 13% value derived from the experimentally determined g_e value.

VII. CONCLUSIONS

The most fundamental magneto-static and electrostatic properties of ThF and ThCl have been experimentally determined. The permanent electric dipole moments are unusually small for a metal halide bond due to polarization of the nonbonding metal centered valence electrons. A high-level of treatment of electron correlation and relativistic effects was required to quantitatively reproduce the ground state dipole moments. The determined g_e values demonstrate that ground

state of ThF is nearly a pure $^2\Delta_{3/2}$, while that for ThCl is more strongly mixed, which is consistent with the weaker electrostatic repulsion due to longer bond distance. As pointed out in Ref.[7], although diatomics such as ThF and ThCl are the simplest molecules in terms of the number of nuclei involved and geometry, they are not necessarily the simplest in terms of electronic structure because, in general, they are not full ligated. These ephemeral molecules are also difficult to generate and detect. As in the case of ThF and ThCl, the non-bonding electrons produce a multitude of low-lying interacting electronic states, which are difficult to model. The qualitative data produced here can be used for accessing the computational methodologies being developed for these simple diatomics as well as more complex actinide containing molecules. Modeling of the excited states and spin-orbit splitting in the ground state of ThF and ThCl remains a major challenge.

Supporting Information

Seven tables labeled S1-S7 . Tables S1-S3 are the observed and calculated field-free, Stark, and Zeeman transition wavenumbers and shifts for the [18.6] Ω=3/2 – $X^2\Delta_{3/2}$(v′,0) band of ThF. Tables S4 and S5 are the observed and calculated field-free for the [18.2] Ω=3/2 – $X^2\Delta_{3/2}$(v′,0) band. of $Th^{35}Cl$ and $Th^{37}Cl$. Tables S6 and S7 are the observed and calculated Stark and Zeeman shifts for the [18.2] Ω=3/2 – $X^2\Delta_{3/2}$(v′,0) band of $Th^{35}Cl$.

Acknowledgment

The research at Arizona State University was supported by a grant from the DoE- Heavy Elements Program (DE-SC0018241). The authors thank Prof. Michael Heaven (Emory University) for his insightful comments.

Figure Captions

Figure 1. The 2D spectrum of the molecules produced in the ablation of thorium with the CF_4/argon mixture in the range of 17,400 to 18,800 cm^{-1}. The horizontal bands of fluorescence are the excitation spectra monitored either on resonance, to higher frequency (Stokes 1-3), or to lower frequency (Anti-Stokes) than that of the laser. The bands at 17700, 17790, 17865, 18030, 18295, 18360 and 18575 cm^{-1} have DLIF spectra (D1-D7) characteristic of ThF. The band at 18327 cm^{-1} has a DLIF spectrum (D8) characteristic of ThO and is the $F^1\Sigma^+ - X^1\Sigma^+(0,0)$ transition. High-resolution spectroscopy was performed on the intense band at 18575 cm^{-1} which is assigned as the [18.6] Ω=3/2 – $X^2\Delta_{3/2}$(v′,0) transition.

Figure 2. Higher resolution DFLIF spectra resulting from pulsed dye laser excitation of the ThF band heads at 17712, 17865 and 18575 cm^{-1}. The spectra have not been corrected for instrumental response sensitivity.

Figure 3. Laser excitation spectra of ThF. Upper panel: the laser excitation spectrum of the [18.6] Ω=3/2 – $X^2\Delta_{3/2}$(v′,0) transition extracted from the 2D spectrum. Lower panel: a portion of the high-resolution, field-free, spectrum of the [18.6] Ω=3/2 – $X^2\Delta_{3/2}$(v′,0) band and associated assignments. The branch features marked with "•" were recorded in the presence of a static electric field (Stark effect) while those with an "♦" were recorded in the presence of a static magnetic field (Zeeman effect).

Figure 4. The R(3/2) (ν=18575.4762 cm^{-1}) line of the [18.6] Ω=3/2 – $X^2\Delta_{3/2}$(v′,0) band of ThF recorded field-free and in the presence of a 1500 V/cm electric field with parallel (ΔM_J =0) and perpendicular (ΔM_J =±1) polarizations. Also shown are the energy level pattern and assignment.

Figure 5. The R(3/2) (ν=18575.4762 cm^{-1}) line of the [18.6] Ω=3/2 – $X^2\Delta_{3/2}$(v′,0) band of ThF recorded field-free and in the presence of a 876 G magnetic field with parallel (ΔM_J =0) and perpendicular (ΔM_J =±1) polarizations. Also shown are the energy level pattern and assignment.

Figure 6. Laser excitation spectra of ThCl. Upper panel: the laser excitation spectrum of the [18.2] Ω=3/2 – $X^2\Delta_{3/2}$(v′,0) transition extracted from the 2D spectrum. Lower panel: a portion of the high-

resolution, field-free, spectrum of the [18.2] **Ω**=3/2 – $X\ ^2\Delta_{3/2}$(v',0) band and associated assignments. The branch features marked with "●" were recorded in the presence of a static electric field (Stark effect) while those with an "♦" were recorded in the presence of a static magnetic field (Zeeman effect). Only the branch labels for $Th^{35}Cl$ are given.

Figure 7. High resolution DLIF spectrum resulting from pulsed dye laser excitation of near the *R*-branch head (ν=18158 cm^{-1}) of the [18.2] **Ω**=3/2 – $X^2\Delta_{3/2}$(v′,0) band of ThCl.

Figure 8. Stark spectra of the *Q*(3/2) line of the ThCl [18.2] **Ω**=3/2 – $X^2\Delta_{3/2}$(v′,0) band recorded in the presence of a 405 V/cm electric field and associated energy levels and assignment. The energy level spacings were obtained using the optimized set of parameters of Table II.

Figure 9. The Zeeman spectra of the *P*(3/2) of the ThCl [18.2] **Ω**=3/2 – $X^2\Delta_{3/2}$(v′,0) band recorded field free and in the presence of a 931G field with parallel and perpendicular polarization and the associated assignment. The energy level spacings were obtained using the optimized set of parameters of Table II.

References

(1) Huang, P.-W.; Wang, C.-Z.; Wu, Q.-Y.; Lan, J.-H.; Song, G.; Chai, Z.-F.; Shi, W.-Q. Understanding Am^{3+}/Cm^{3+} Separation with H_4TPAEN and its Hydrophilic Derivatives: a Quantum Chemical Study. *Phys. Chem. Chem. Phys.* **2018,** *20* (20), 14031-14039.

(2) Kong, X.-H.; Wu, Q.-Y.; Wang, C.-Z.; Lan, J.-H.; Chai, Z.-F.; Nie, C.-M.; Shi, W.-Q. Insight into the Extraction Mechanism of Americium (III) over Europium (III) with Pyridylpyrazole: A Relativistic Quantum Chemistry Study. *J. Phys. Chem. A* **2018,** *122* (18), 4499-4507.

(3) Leoncini, A.; Huskens, J.; Verboom, W. Ligands for f-Element Extraction Used in the Nuclear Fuel Cycle. *Chem. Soc. Rev.* **2017,** *46* (23), 7229-7273.

(4) Afsar, A.; Distler, P.; Harwood, L. M.; John, J.; Westwood, J. Extraction of Minor Actinides, Lanthanides and Other Fission Products by Silica-immobilized BTBP/BTPhen Ligands. *Chem. Comm.* **2017,** *53* (28), 4010-4013.

(5) Gorden, A. E. V.; DeVore, M. A.; Maynard, B. A. Coordination Chemistry with f-Element Complexes for an Improved Understanding of Factors That Contribute to Extraction Selectivity. *Inor. Chem.* **2013,** *52* (7), 3445-3458.

(6) Heaven, M. C.; Barker, B. J.; Antonov, I. O. Spectroscopy and Structure of the Simplest Actinide Bonds. *J. Phys. Chem. A* **2014,** *118* (46), 10867-10881.

(7) Heaven, M. C.; Barker, B. J.; Antonov, I. O. Correction to Spectroscopy and Structure of the Simplest Actinide Bonds. *J. Phys. Chem. A* **2015,** *119* (41), 10440-10440.

(8) Kaledin, L. A.; McCord, J. E.; Heaven, M. C. Laser Spectroscopy of UO: Characterization and Assignment of States in the 0-to 3-eV Range, with a Comparison to the Electronic Structure of ThO. *J. Mol. Spectrosc.* **1994,** *164* (1), 27-65.

(9) Field, R. W. Diatomic Molecule Electronic Structure Beyond Simple Molecular Constants. *Berichte der Bunsengesellschaft für physikalische Chemie* **1982,** *86* (9), 771-779.

(10) Barker, B. J.; Antonov, I. O.; Heaven, M. C.; Peterson, K. A. Spectroscopic Investigations of ThF and ThF^+. *J. Chem. Phys.***2012,** *136* (10), 104305.

(11) Bross, D. H.; Peterson, K. A. Theoretical Spectroscopy Study of the Low-Lying Electronic States of UX and UX^+, X= F and Cl. *J. Chem. Phys.* **2015,** *143* (18), 184313.

(12) VanGundy, R. A.; Bartlett, J. H.; Heaven, M. C.; Battey, S. R.; Peterson, K. A. Spectroscopic and Theoretical Studies of ThCl and $ThCl^+$. *J. Chem. Phys.* **2017,** *146* (5), 054307.

(13) Schall, H.; Gray, J.; Dulick, M.; Field, R. Sub-Doppler Zeeman spectroscopy of the CeO molecule. *J. Chem. Phys.* **1986,** *85* (2), 751-762.

(14) Heaven, M. C.; Goncharov, V.; Steimle, T. C.; Ma, T.; Linton, C. The Permanent Electric Dipole Moments and Magnetic g-Factors of Uranium Monoxide. *J. Chem. Phys.* **2006,** *125* (20), 204314.

(15) Linton, C.; Adam, A.; Steimle, T. Stark and Zeeman Effect in the [18.6] 3.5–X (1) 4.5 Transition of Uranium Monofluoride, UF. *J. Chem. Phys.***2014,** *140* (21), 214305.

(16) Jung, J.; Atanasov, M.; Neese, F. Ab Initio Ligand-Field Theory Analysis and Covalency Trends in Actinide and Lanthanide Free Ions and Octahedral Complexes. *Inor. Chem.* **2017,** *56* (15), 8802-8816.

(17) Matthew, D. J.; Morse, M. D. Resonant Two-Photon Ionization Spectroscopy of Jet-Cooled UN: Determination of the Ground State. *J. Chem. Phys.* **2013,** *138* (18), 184303.

(18) Irikura, K. K. Gas-Phase Energetics of Thorium Fluorides and Their Ions. *J. Phys. Chem. A* **2012,** *117* (6), 1276-1282.

(19) Thanthiriwatte, K. S.; Wang, X.; Andrews, L.; Dixon, D. A.; Metzger, J.; Vent-Schmidt, T.; Riedel, S. Properties of ThF_x from Infrared Spectra in Solid Argon and Neon with Supporting Electronic Structure and Thermochemical Calculations. *J. Phys. Chem. A* **2014,** *118* (11), 2107-2119.

(20) Kokkin, D. L.; Steimle, T. C.; DeMille, D. Branching Ratios and Radiative Lifetimes of the U, L, and I States of Thorium Oxide. *Phy. Rev. A* **2014,** *90* (6), 062503.

(21) Kokkin, D. L.; Steimle, T. C.; DeMille, D. Characterization of the I(| Ω|= 1)–X $^1\Sigma^+$(0, 0) Band of Thorium Oxide. *Phy. Rev. A* **2015,** *91* (4), 042508.

(22) Steimle, T. C.; Zhang, R.; Heaven, M. C. The Pure Rotational Spectrum of Thorium Monosulfide, ThS. *Chem.Phys. Lett.* **2015,** *639*, 304-306.

(23) Le, A.; Heaven, M. C.; Steimle, T. C. The Permanent Electric Dipole Moment of Thorium Sulfide, ThS. *J. Chem. Phys.* **2014,** *140* (2), 024307.

(24) Gascooke, J. R.; Alexander, U. N.; Lawrance, W. D. Two Dimensional Laser Induced Fluorescence Spectroscopy: A Powerful Technique for Elucidating Rovibronic Structure in Electronic Transitions of Polyatomic Molecules. *J. Chem. Phys.* **2011,** *134* (18), 184301.

(25) Reilly, N. J.; Schmidt, T. W.; Kable, S. H. Two-Dimensional Fluorescence (Excitation/Emission) Spectroscopy as a Probe of Complex Chemical Environments. *J. Phys. Chem. A* **2006,** *110* (45), 12355-12359.

(26) Raghavachari, K.; Trucks, G. W.; Pople, J. A.; Head-Gordon, M. A Fifth-Order Perturbation Comparison of Electron Correlation Theories. *Chem. Phys. Lett.* **1989,** *157* (6), 479-483.

(27) Liu, J.; Cheng, L. An Atomic Mean-Field Spin-Orbit Approach within Exact Two-Component Theory for a Non-Perturbative Treatment of Spin-Orbit Coupling. *J. Chem. Phys.* **2018,** *148* (14), 144108.

(28) Dyall, K. G. Interfacing Relativistic and Nonrelativistic Methods. I. Normalized Elimination of the Small Component in the Modified Dirac Equation. *J. Chem. Phys.* **1997,** *106* (23), 9618-9626.

(29) Kutzelnigg, W.; Liu, W. Quasirelativistic Theory Equivalent to Fully Relativistic Theory. *J. Chem. Phys.* **2006,** *125* (10), 107102.

(30) Iliaš, M.; Saue, T. An Infinite-Order Two-Component Relativistic Hamiltonian by a Simple One-Step Transformation. *J. Chem. Phys.* **2007,** *126* (6), 064102.

(31) Hess, B. A.; Marian, C. M.; Wahlgren, U.; Gropen, O. A Mean-Field Spin-Orbit Method Applicable to Correlated Wavefunctions. *Chem.Phys. Lett.* **1996,** *251* (5-6), 365-371.

(32) Fægri Jr, K.; Visscher, L. Relativistic Calculations on Thallium Hydride. *Theor.Chem. Acc.* **2001,** *105* (3), 265-267.

(33) Roos, B. O.; Lindh, R.; Malmqvist, P.-Å.; Veryazov, V.; Widmark, P.-O. New Relativistic ANO Basis Sets for Transition Metal Atoms. *J. Phys. Chem. A* **2005,** *109* (29), 6575-6579.

(34) Liu, J.; Shen, Y.; Asthana, A.; Cheng, L. Two-Component Relativistic Coupled-Cluster Methods Using Mean-Field Spin-Orbit Integrals. *J. Chem. Phys.* **2018,** *148* (3), 034106.

(35) Noga, J.; Bartlett, R. J. The Full CCSDT Model for Molecular Electronic Structure. *J. Chem. Phys.***1987,** *86* (12), 7041-7050.

(36) Scuseria, G. E.; Schaefer III, H. F. A New Implementation of the Full CCSDT Model for Molecular Electronic Structure. *Chem.Phys. Lett.* **1988,** *152* (4-5), 382-386.

(37) Bomble, Y. J.; Stanton, J. F.; Kállay, M.; Gauss, J. Coupled-Cluster Methods Including Noniterative Corrections for Quadruple Excitations. *J. Chem. Phys.* **2005,** *123* (5), 054101.

(38) Dyall, K. G. Interfacing Relativistic and Nonrelativistic Methods. IV. One-and Two-Electron Scalar Approximations. *J. Chem. Phys.* **2001,** *115* (20), 9136-9143.

(39) Liu, W.; Peng, D. Exact Two-Component Hamiltonians Revisited. *J. Chem. Phys.* **2009,** *131* (3), 031104.

(40) Cheng, L.; Gauss, J. Analytic Energy Gradients for the Spin-Free Exact Two-Component Theory Using an Exact Block Diagonalization for the One-Electron Dirac Hamiltonian. *J. Chem. Phys.* **2011,** *135* (8), 084114.

(41) Dunning Jr, T. H. Gaussian Basis Sets for Use in Correlated Molecular Calculations. I. The Atoms Boron through Neon and Hydrogen. *J. Chem. Phys.* **1989,** *90* (2), 1007-1023.

(42) Feng, R.; Peterson, K. A. Correlation Consistent Basis Sets for Actinides. II. The Atoms Ac and Np–Lr. *J. Chem. Phys.* **2017,** *147* (8), 084108.

(43) Stanton, J.; Gauss, J.; Harding, M.; Szalay, P.; Auer, A.; Bartlett, R.; Benedikt, U.; Berger, C.; Bernholdt, D.; Bomble, Y. CFOUR, Coupled-Cluster Techniques for Computational Chemistry, a Quantum-Chemical Program Package. *Current version available at http://www. cfour. de* **2009**.

(44) Stanton, J. F.; Gauss, J.; Watts, J. D.; Bartlett, R. J. A Direct Product Decomposition Approach for Symmetry Exploitation in Many-Body Methods. I. Energy cCalculations. *J. Chem. Phys.* **1991,** *94* (6), 4334-4345.

(45) Watts, J. D.; Gauss, J.; Bartlett, R. J. Coupled-Cluster Methods with Noniterative Triple Excitations for Restricted Open-Shell Hartree-Fock and Other General Single Determinant Reference Functions. Energies and Analytical Gradients. *J. Chem. Phys.* **1993,** *98* (11), 8718-8733.

(46) Kállay, M.; Rolik, Z.; Csontos, J.; Ladjánszki, I.; Szegedy, L.; Ladóczki, B.; Samu, G.; Petrov, K.; Farkas, M.; Nagy, P. MRCC, a Quantum Chemical Program Suite. *See also: http://www.mrcc.hu* **2015**.

(47) Kállay, M.; Surján, P. R. Higher Excitations in Coupled-Cluster Theory. *J. Chem. Phys.* **2001,** *115* (7), 2945-2954.

(48) Kállay, M.; Gauss, J. Approximate Treatment of Higher Excitations in Coupled-Cluster theory. *J. Chem. Phys.* **2005,** *123* (21), 214105.

(49) Edvinsson, G.; Selin, L.-E.; Aslund, N. On the Band Spectrum of ThO. *Arkiv Fys.* **1965,** *30*.

(50) Brown, J.; Cheung, A.-C.; Merer, A. Λ-type Doubling Parameters for Molecules in Δ Electronic States. *J. Mol. Spectrosc.* **1987,** *124* (2), 464-475.

(51) Brown, J. M.; Carrington, A., *Rotational Spectroscopy of Diatomic Molecules*. Cambridge University Press: Cambridge, U.K., 2003.

(52) Qin, C.; Linton, C.; Steimle, T. C. Optical Zeeman Spectroscopy of the (0, 0) $B^4\Gamma$–$X^4\Phi$ Band Systems of Titanium Monohydride, TiH, and Titanium Monodeuteride, TiD. *J. Chem. Phys.* **2012,** *137* (7), 074301.

(53) Dewberry, C. T.; Etchison, K. C.; Cooke, S. A. The Pure Rotational Spectrum of the Actinide-Containing Compound Thorium Monoxide. *Phys. Chem. Chem. Phys.* **2007,** *9* (35), 4895-4897.

Table 1. Spectroscopic parameters for [18.6] **Ω**=3/2 – $X^2\Delta_{3/2}$(v′,0) transition of ThF.

	[18.2] Ω=3/2	$X^2\Delta_{3/2}$(v=0)
Field-free		
B [a]	0.217115(8)	0.233031(9)
T_0 [b]	18574.42255 (12)	
σ [c]	0.00032	
Stark		
$\lvert\mu_{el}\rvert$	0.589(10) D	1.453(7) D
σ	0.00020	
Zeeman		
g_S	2.0023(fix)	2.0023(fix)
g_L [d]	1.079(4)	1.038(4)
g_e	1.156(4)	1.075(4)
σ	0.00033	

a) B, T_0 and σ in units of wavenumber (cm^{-1}). $\lvert\mu_{el}\rvert$ in units of Debye (D). The numbers in parentheses represent a 2σ error estimate.

b) The spin-orbit parameters, A, of the $X^2\Delta_{3/2}$(v=0) and [18.2] $^2\Delta_{3/2}$ states constrained to 1749 cm^{-1}.

c) Standard deviation of the fit.

d) Value obtained assuming a $^2\Delta$ state designation.

Table 2. Spectroscopic parameters for [18.2] Ω=3/2 – $X^2\Delta_{3/2}$(v′,0) transition of ThCl.

	[18.2] Ω=3/2		$X^2\Delta_{3/2}$(v=0)	
Field-free				
	$Th^{35}Cl$	$Th^{37}Cl$	$Th^{35}Cl$	$Th^{37}Cl$
B [a]	0.084690(7)	0.080814(9)	0.088671(7)	0.084510(9)
$(p_\Delta+4q_\Delta)$ $(\times10^{-5})$	-3.6338(10)	-3.3078(30)		
T_0 [b]	18156.71516(17)	18156.78696(20)		
σ [c]	0.00066	0.00058		
Stark				
$\lvert\mu_{el}\rvert$	3.020(6) D		2.022(35) D	
σ	0.00030			
Zeeman				
g_S	2.0023(fix)		2.0023(fix)	
g_L [d]	1.320(4)		1.063(4)	
g_e	1.638(4)		1.130(4)	
σ	0.00037			

a) B, $(p_\Delta+4q_\Delta)$, T_0 and σ in units of wavenumber (cm^{-1}). $\lvert\mu_{el}\rvert$ in units of Debye (D). The numbers in parentheses represent a 2σ error estimate.

b) The spin-orbit parameters, A, of the $X^2\Delta_{3/2}$(v=0) and [18.2] $^2\Delta_{3/2}$ states constrained to 1749 cm^{-1}.

c) Standard deviation of the fit.

d) Value obtained assuming a $^2\Delta$ state designation.

Table 3. Calculated ground state dipole moments.

	X2CAMF-HF	X2CAMF-CCSD [a]	X2CAMF-CCSD(T)	+ΔT[b]	+ΔQ[c]	Exp.
ThF	-0.018	1.275 (-12.2%)	1.504 (3.5%)	1.431 (-1.5%)	1.376 (-5.3%)	1.453(7)
ThCl	0.643	1.957 (-3.2%)	2.245 (11.0%)	2.124 (5.0%)	2.035 (0.6%)	2.022(35)

a) The percentage difference to the experimental values are given in parentheses.

b) Obtained using SFX2C-1e-CCSDT.

c) Obtained using SFX2C-1e-CCSDT(Q)

Table 4. Dipole moments of ThX(X=F, Cl, O, S) and UF.

	ThF ($X\,^2\Delta_{3/2}$)	ThCl($X\,^2\Delta_{3/2}$)	ThO ($X\,^1\Sigma^+$)	ThS($X\,^1\Sigma^+$)	UF(X(1)4.5)
$\lvert\mu_{el}\rvert$ (D)	1.453	2.022	2.022	4.58	2.01
R_e(Å)	2.02937	2.5009	1.84018	2.3436	2.030 Å
$\lvert\mu_{el}\rvert/R_e$ (D/ Å)	0.7026	0.8085	1.0988	1.95	0.99
q(eff) [a]	0.146e	0.168e	0.229e	0.406e	0.206e
Config.	$Th^+(7s^26d^1)$	$Th^+(7s^26d^1)$	$Th^{2+}(7s^2)$	$Th^{2+}(7s^2)$	$U^+(5f^3\,7s^2)$
Δ(Elec. Neg.)[b]	2.68	1.86	2.14	1.28	2.60

a) The effective point charge need to reproduce the observed $\lvert\mu_{el}\rvert$ for the observed bond distances.

b) Difference in electronegativity between the ligand and the metal.

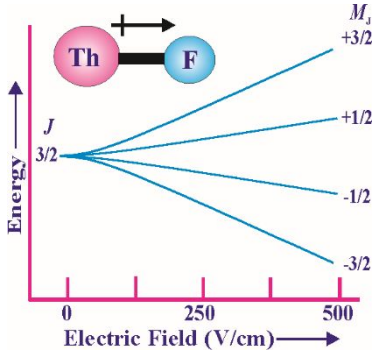
Th
F
M_J
+3/2
+1/2
-1/2
-3/2
J
3/2
Energy
0
250
500
Electric Field (V/cm)

Figure 1

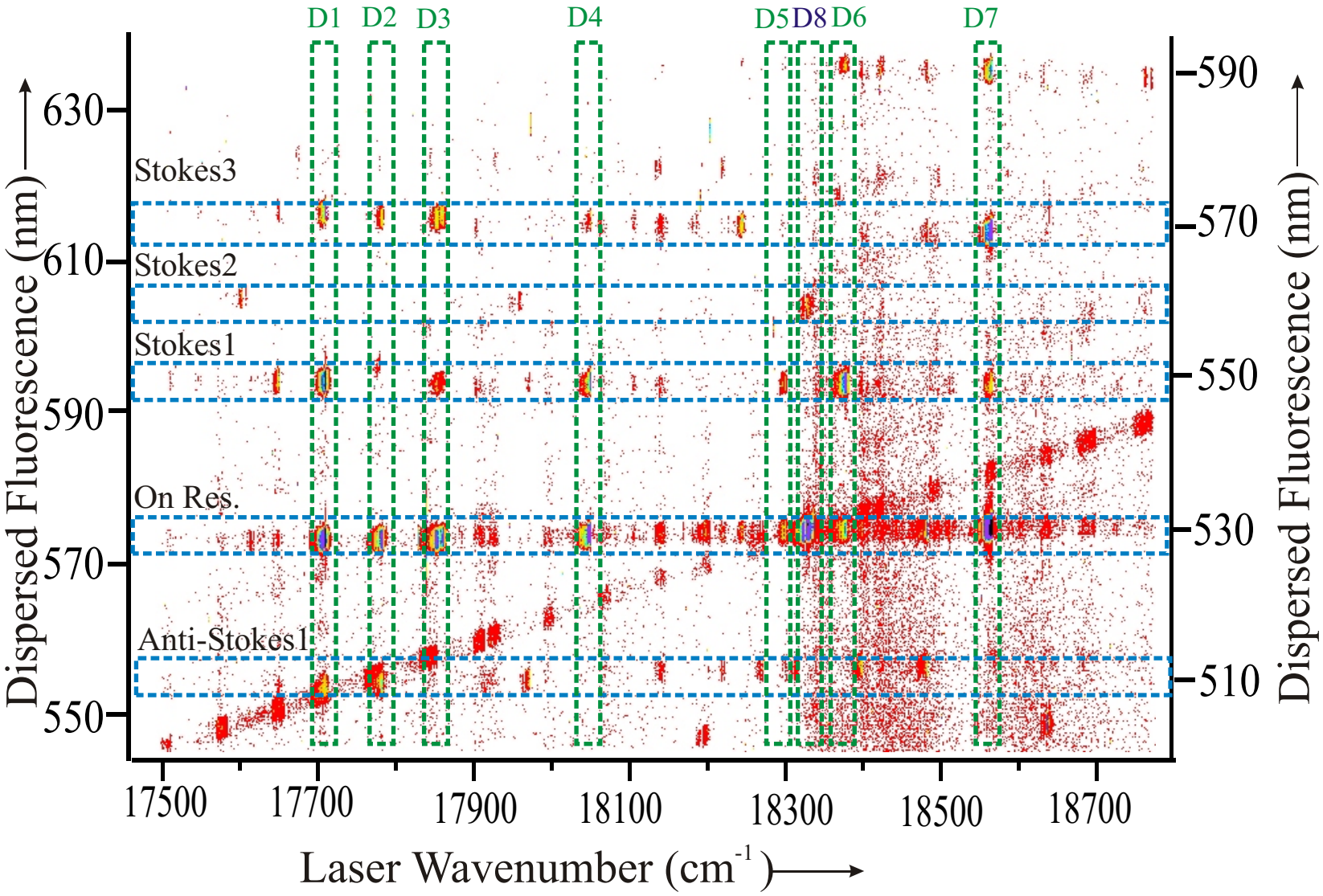
D1
D2
D3
D4
D5
D8
D6
D7
Stokes3
Stokes2
Stokes1
On Res.
Anti-Stokes1
Dispersed Fluorescence (nm)
630
610
590
570
550
590
570
550
530
510
Dispersed Fluorescence (nm)
17500
17700
17900
18100
18300
18500
18700
Laser Wavenumber (cm-1)

Figure 2

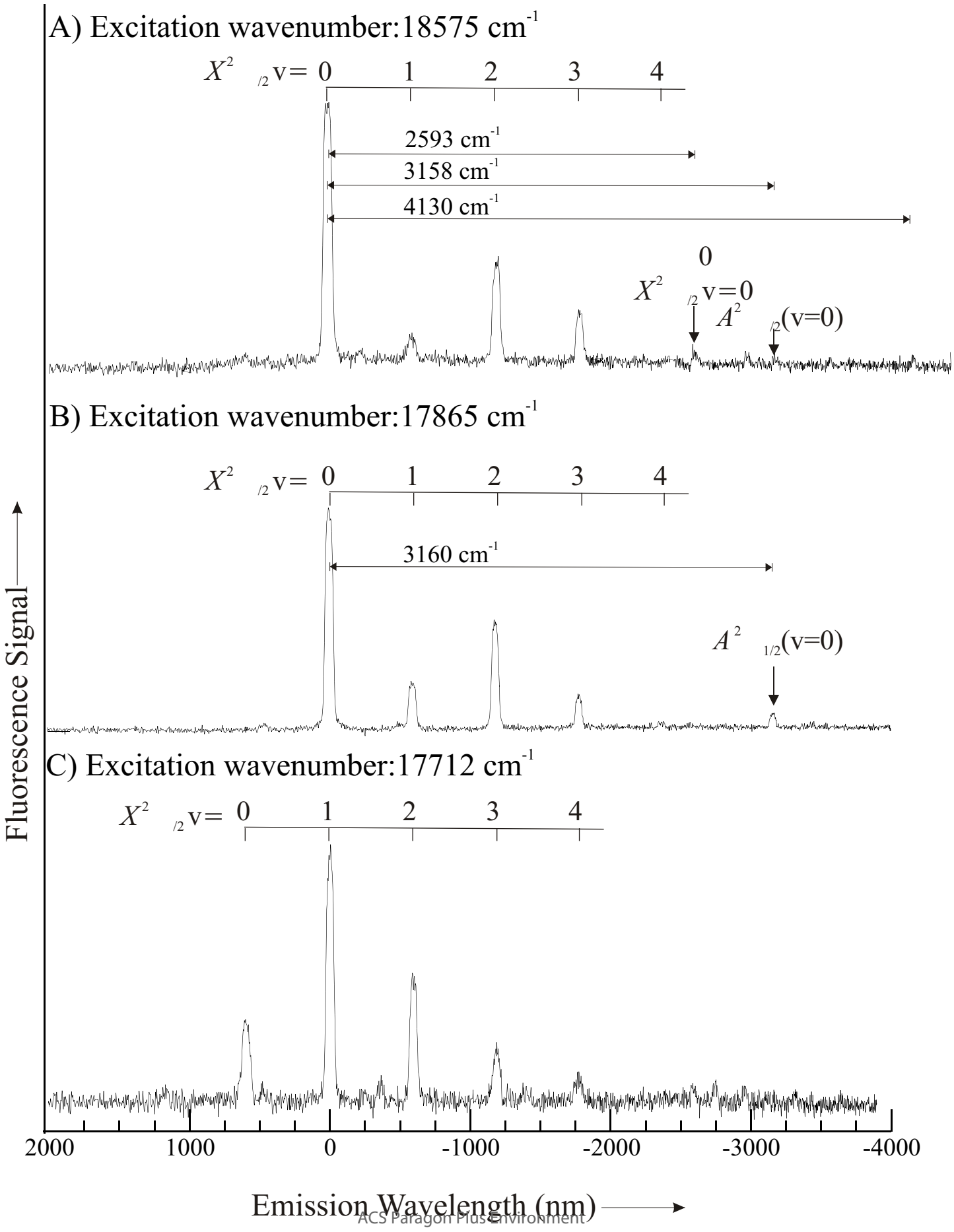
A) Excitation wavenumber:18575 cm-1
X2 /2 v= 0 1 2 3 4
2593 cm-1
3158 cm-1
4130 cm-1
0
X2 /2 v=0
A2 /2(v=0)
B) Excitation wavenumber:17865 cm-1
X2 /2 v= 0 1 2 3 4
3160 cm-1
A2 1/2(v=0)
C) Excitation wavenumber:17712 cm-1
X2 /2 v= 0 1 2 3 4
Fluorescence Signal
2000 1000 0 -1000 -2000 -3000 -4000
Emission Wavelength (nm)

Figure 3

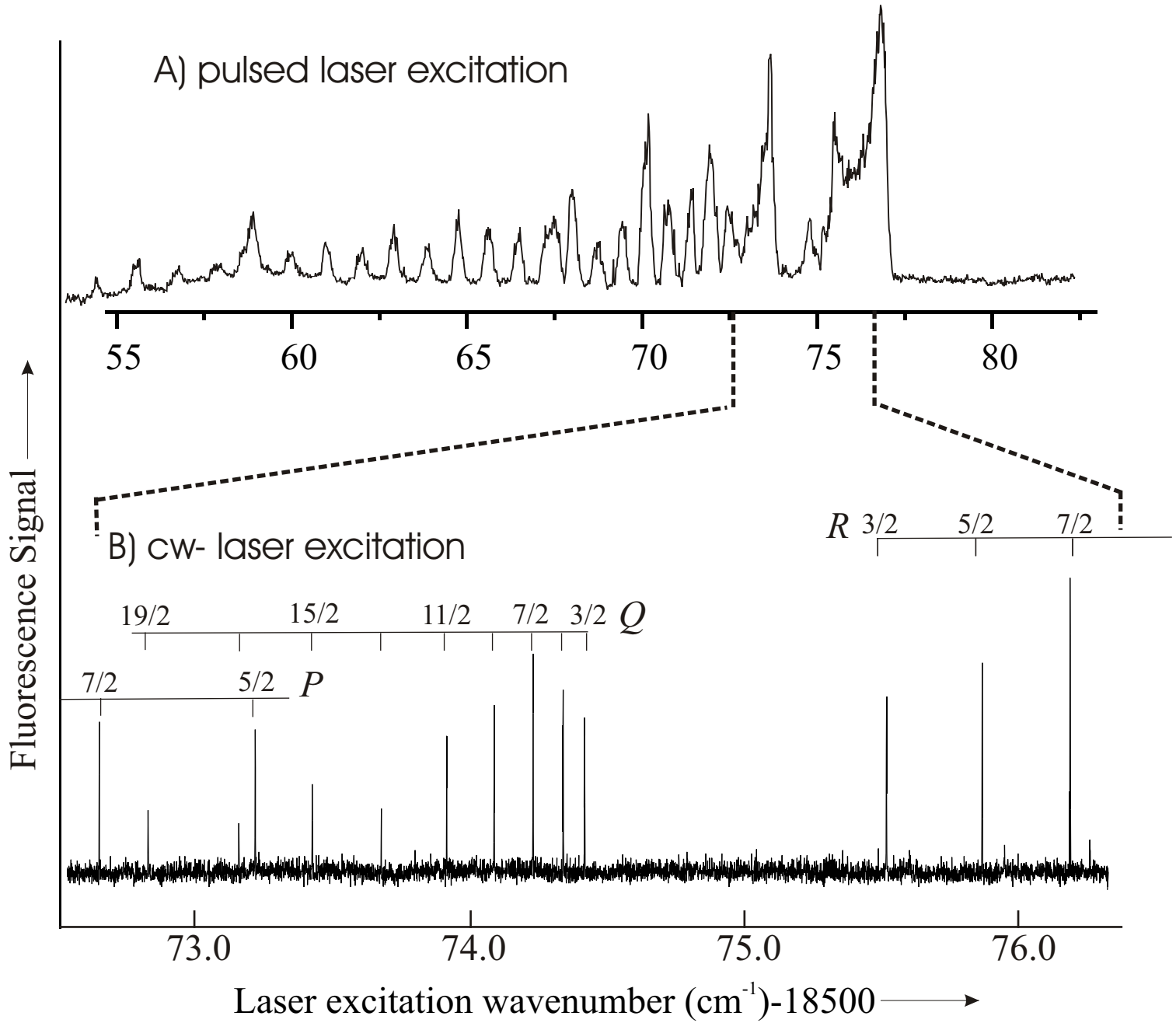
A) pulsed laser excitation
55
60
65
70
75
80
B) cw- laser excitation
R 3/2 5/2 7/2
19/2 15/2 11/2 7/2 3/2 Q
7/2 5/2 P
Fluorescence Signal
73.0
74.0
75.0
76.0
Laser excitation wavenumber (cm-1)-18500

Figure 4

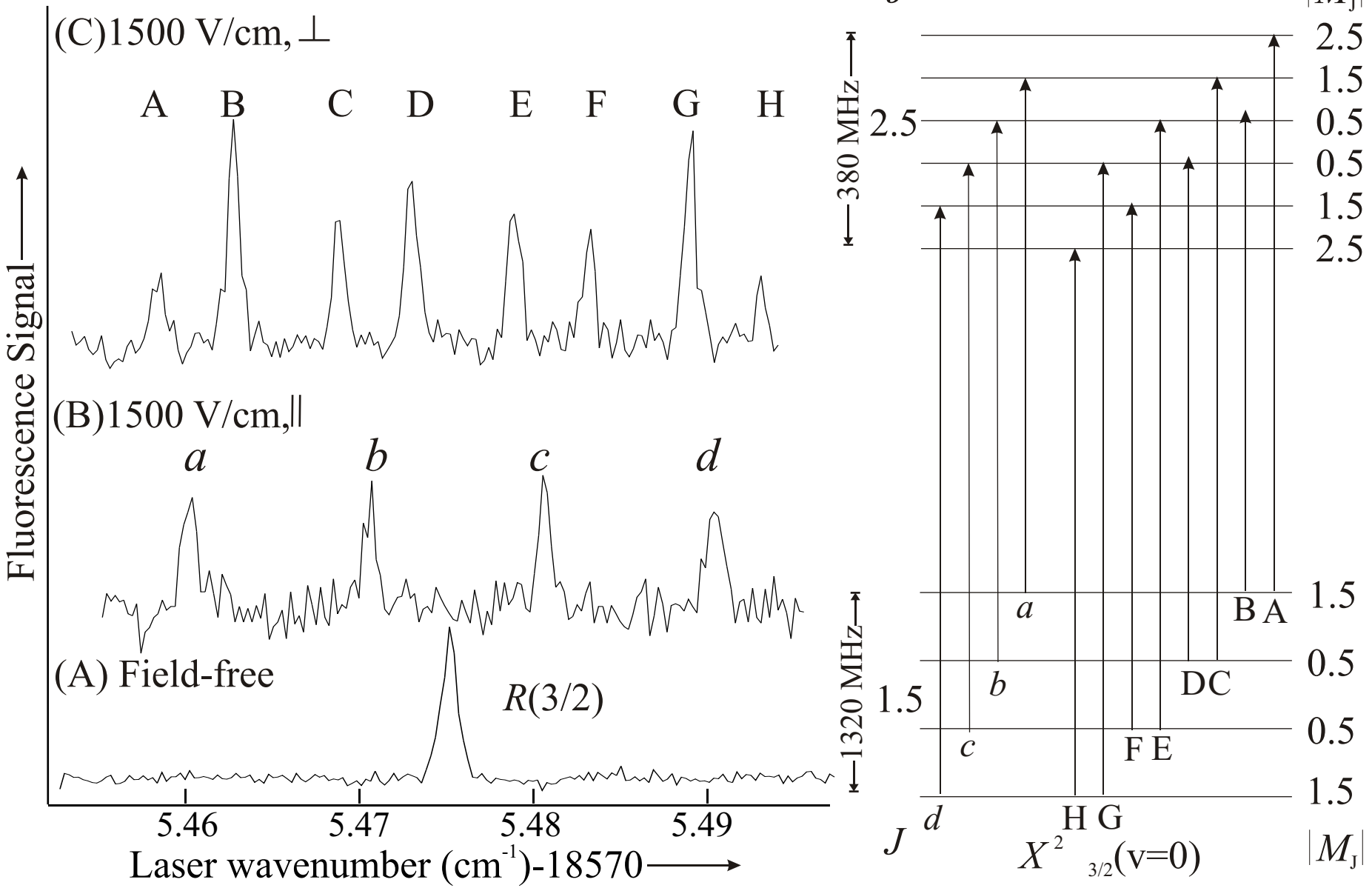
(C)1500 V/cm, ⊥
A B C D E F G H
(B)1500 V/cm, ||
a b c d
(A) Field-free
R(3/2)
Fluorescence Signal
5.46 5.47 5.48 5.49
Laser wavenumber (cm-1)-18570
J
[18.6] =3/2
|MJ|
380 MHz
2.5
2.5 1.5 0.5 0.5 1.5 2.5
1320 MHz
1.5
1.5 0.5 0.5 1.5
a b c d
B A DC F E H G
J
X 2 3/2(v=0)

Figure 5

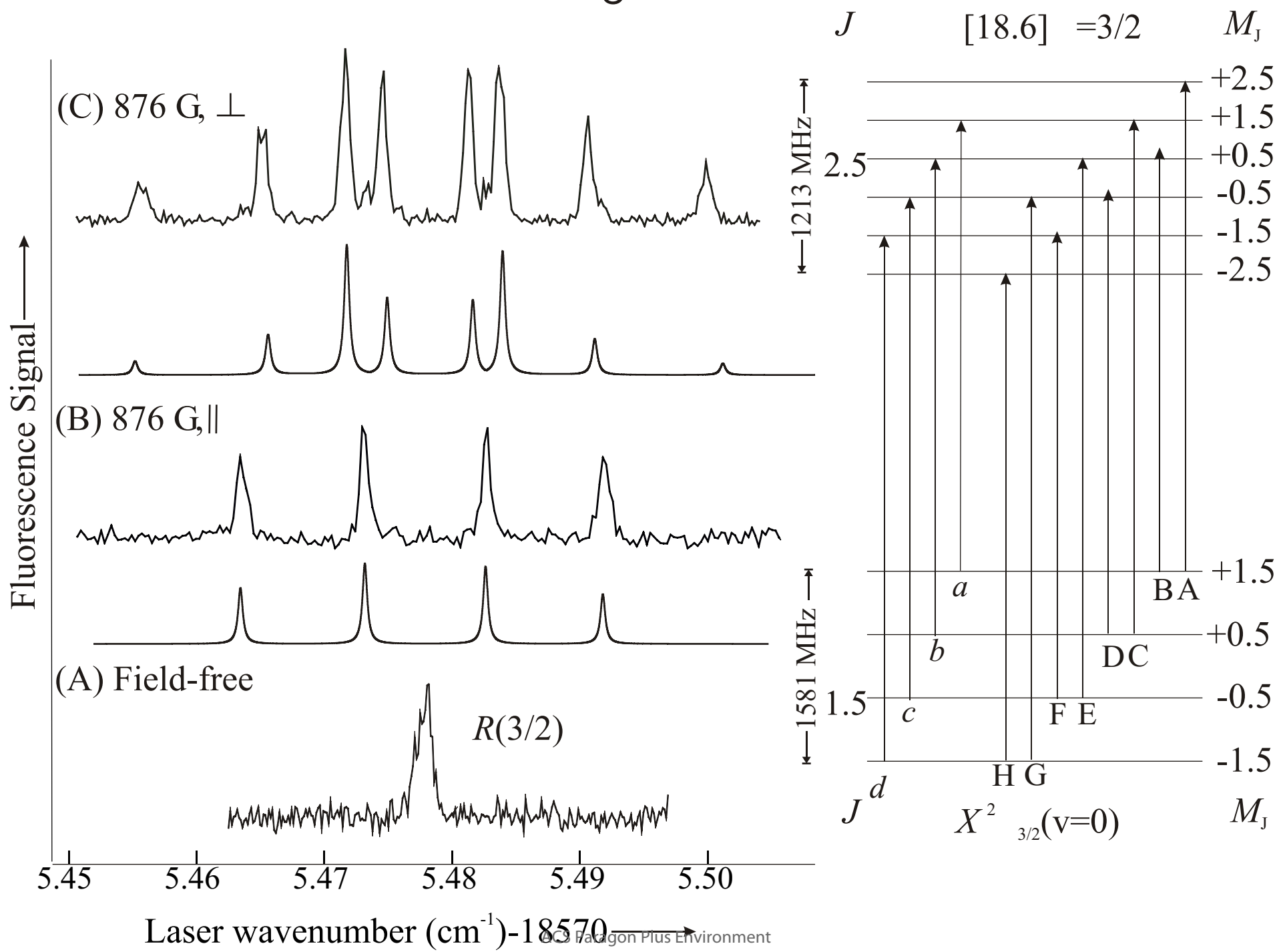

Figure 6

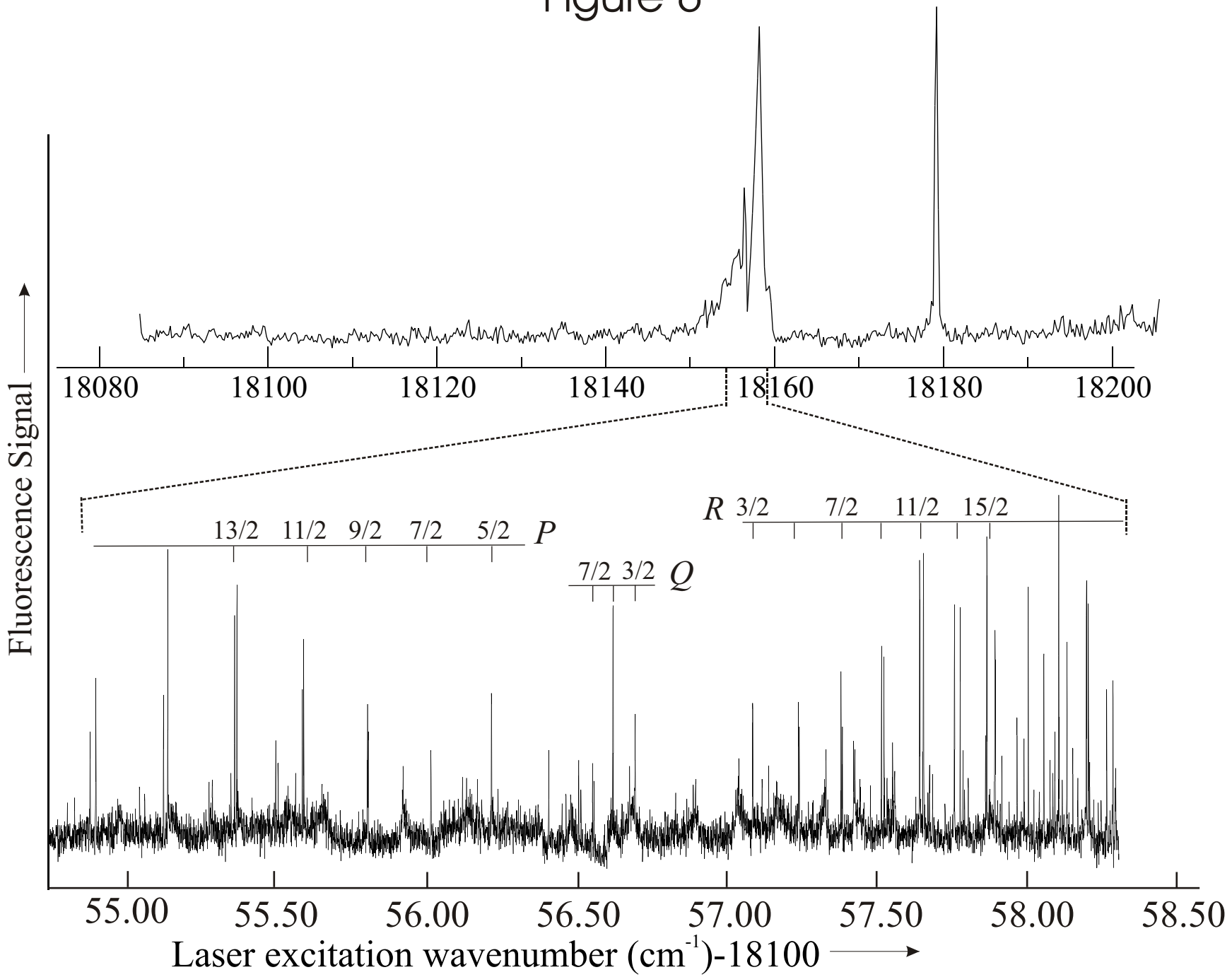
Fluorescence Signal
18080
18100
18120
18140
18160
18180
18200
13/2 11/2 9/2 7/2 5/2 P
7/2 3/2 Q
R 3/2 7/2 11/2 15/2
55.00
55.50
56.00
56.50
57.00
57.50
58.00
58.50
Laser excitation wavenumber (cm-1)-18100

Figure 7

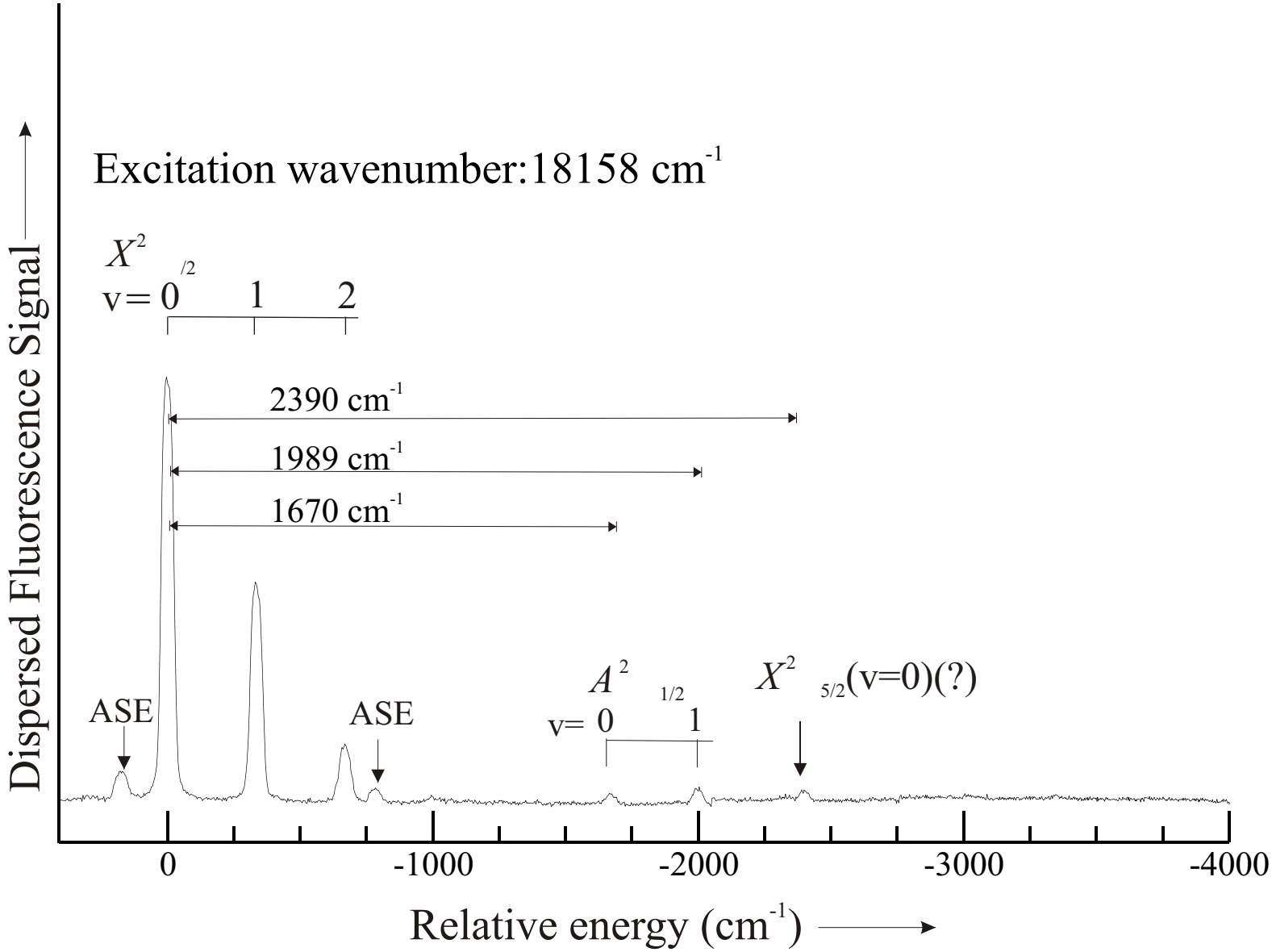
Excitation wavenumber:18158 cm-1
X2
v= 0 1 2
/2
2390 cm-1
1989 cm-1
1670 cm-1
ASE
ASE
A 2
1/2
v= 0 1
X2
5/2(v=0)(?)
Dispersed Fluorescence Signal
0
-1000
-2000
-3000
-4000
Relative energy (cm-1)

Figure 8

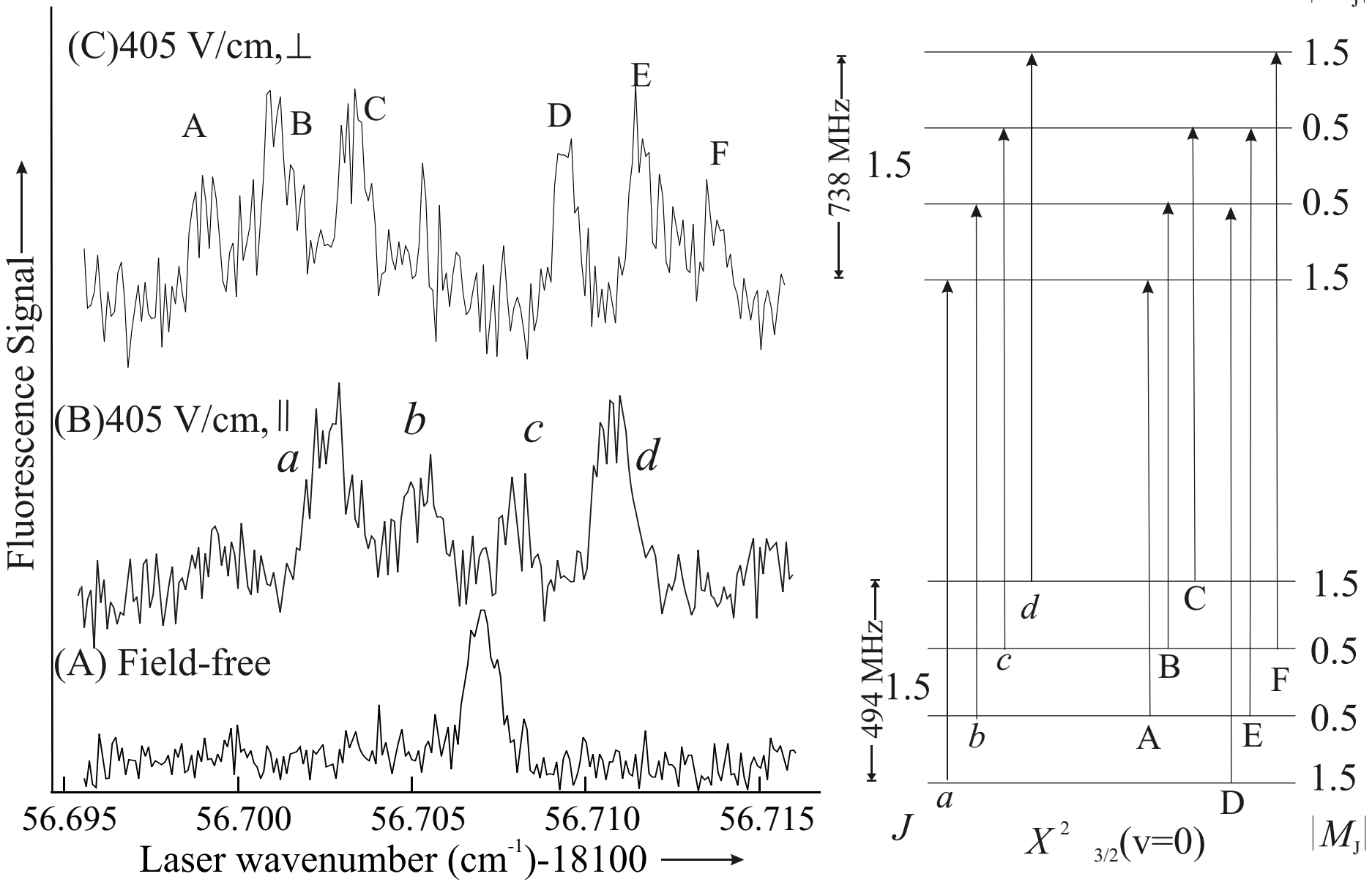
(C)405 V/cm,⊥
A
B
C
D
E
F
(B)405 V/cm, ||
a
b
c
d
(A) Field-free
Fluorescence Signal
56.695
56.700
56.705
56.710
56.715
Laser wavenumber (cm-1)-18100
J
[18.2] =3/2
|MJ|
738 MHz
1.5
1.5
0.5
0.5
1.5
494 MHz
1.5
1.5
0.5
0.5
1.5
a
b
c
d
A
B
C
D
E
F
J
X 2 3/2(v=0)
|MJ|

Figure 9